

Fate and transformation products of amine-terminated PAMAM dendrimers under ozonation and irradiation

This version is made available in accordance with publisher policies.

Please, cite as follows:

Javier Santiago-Morales, Roberto Rosal, María D. Hernando, Maria M. Ulaszewska, Eloy García-Calvo, Amadeo R. Fernández-Alba, Fate and transformation products of amine-terminated PAMAM dendrimers under ozonation and irradiation, *Journal of Hazardous Materials*, Volume 266, 15 February 2014, Pages 102-113, <http://dx.doi.org/10.1016/j.jhazmat.2013.12.021>.

Fate and transformation products of amine-terminated PAMAM dendrimers under ozonation and irradiation

Javier Santiago-Morales¹, Roberto Rosal^{1,2,*}, María D. Hernando³, Maria M. Ulaszewska^{2,‡}, Eloy García-Calvo^{1,2}, Amadeo R. Fernández-Alba^{2,4}

1 Department of Chemical Engineering, University of Alcalá, 28871 Alcalá de Henares, Madrid, Spain

2 Advanced Study Institute of Madrid, IMDEA Agua, Parque Científico Tecnológico, 28805 Alcalá de Henares, Madrid, Spain

3 Spanish National Institute for Agricultural and Food Research and Technology - INIA, Crta. de la Coruña, km 7.5, 28040, Madrid, Spain

4 Pesticide Residue Research Group, Department of Hydrogeology and Analytical Chemistry, University of Almería, 04120, Almería, Spain

* Corresponding author: roberto.rosal@uah.es

‡ Current address: Department of Food Quality and Nutrition, Research and Innovation Centre, Fondazione Edmund Mach, San Michele all'Adige, Italy.

Abstract

This article deals with the degradation of a third-generation (G3) poly(amidoamine) (PAMAM) dendrimer under ozonation and irradiation. The identification and quantification of G3 PAMAM dendrimer and its transformation products has been performed by liquid chromatography–electrospray ionization–hybrid quadrupole time-of-flight–mass spectrometry. The dendrimer was completely depleted by ozone in less than 1 min. The effect of ultraviolet irradiation was attributed to hydroxyl-mediated oxidation. The transformation products were attributed to the oxidation of amines, which resulted in highly oxidized structures with abundance of carboxylic acids, which started from the formation of amine oxide and the scission of the C-N bond of the amide group. We studied the toxicity of treated mixtures for six different organisms: the acute toxicity for the bacterium *Vibrio fischeri* and the microcrustacean *Daphnia magna*, the multigenerational growth inhibition of the alga *Pseudokirchneriella subcapitata*, and the seed germination phytotoxicity of *Licopersicon esculentum*, *Lactuca sativa* and *Lolium perenne*. Ozonation and irradiation originated transformation products are more toxic than the parent dendrimer. The toxicity of the dendrimer for the green alga was linked to a strong increase of intracellular reactive oxygen species with intense lipid peroxidation.

Keywords: PAMAM dendrimer, ozonation, ultraviolet irradiation, transformation products, liquid chromatography–electrospray ionization quadrupole/time-of-flight mass spectrometry

1. Introduction

The use of manufactured nanomaterials has been rapidly increasing during the last years in a wide variety of applications making it necessary more extensive toxicology measurements and risk assessment studies [1]. This work focuses on dendrimers, which are hyperbranched nanoscale polymers with uniform size, defined molecular weight, large internal cavities and a high number of surface groups that make them particularly tunable in terms of solution chemistry [2]. These features make them suitable for several applications such as pharmaceutical and cosmetic additives, drug vectors or analytical carriers [3].

The occurrence of dendrimers in the environment has not yet been reported and therefore there are no data on their concentrations in wastewater or receiving bodies. It is interesting to note that current analytical techniques do not allow the quantification of dendrimers in aqueous matrixes within the range of environmental

concentrations of most anthropogenic pollutants [4]. Consequently, they are likely to be detected with the progress of analytical techniques in view of their expanding range of applications and their excretion profiles. It has been reported that the elimination of certain PAMAM dendrimers in mice takes place mainly via urine [5]. The same has been observed for macromolecular contrast agents based on PAMAM and particularly for the lower generations [6,7]. In this context “generation”, usually abbreviated as “G”, refers to the number of repeated branching cycles performed during synthesis and, consequently, higher generations have higher molecular weight and molecular size. It is generally concluded that generation number and surface charge determine not only the type and rate of excretion, but also the toxicity profile of dendrimers and their conjugates [8].

The toxicity of PAMAM dendrimers is higher for dendrimers of higher generations, which bear a larger

positive charge [9]. Surface modification is a well-known method for charge neutralization and represents a way to modulate cellular uptake and cytotoxicity due to their lower electrostatic interaction with negatively charged cell membranes [10,11]. The toxicity of dendrimers has been linked to the generation of reactive oxygen species (ROS), which would be involved in the disruption of the mitochondrial electron transduction chain, DNA damage and cell apoptosis [12,13]. The ecotoxicity of PAMAM dendrimers is limited to very few studies, which reported EC50 ranging from 0.13 μM of G6 PAMAM (*Daphnia magna*, 48 h) to 194 μM of G2 PAMAM (*Vibrio fischeri*, 30 min) [14].

Once released to the environment, dendrimers would undergo transformation by biotic and abiotic processes, which may alter their fate, transport, and toxicity. The nature and extent of such transformations must be understood in order to make significant progresses toward understanding the environmental risks posed by these materials [15]. Concerning the later, irradiation and oxidation are commonly used in water reuse scenarios in order to reduce the concentrations of germs and micropollutants [16]. We paid special attention to the generation of transformation products (TP) and the toxicity associated with their mixtures, the rationale being that it has been observed that TP of organic pollutants are often more toxic than their parent compounds [17,18]. The identification of G3 dendrimer and its TP has been performed by liquid chromatography–electrospray ionization–hybrid quadrupole time-of-flight–mass spectrometry (LC–ESI–QTOF–MS).

The aim of this work was to explore the effect of ozonation and germicidal ultraviolet (UV, 254 nm) on the fate and G3 amine-terminated PAMAM dendrimer. We also studied its photochemical stability under visible light irradiation in order to approximate the situation that could take place in aquatic ecosystems. The toxicity assessment of treated mixtures was conducted using six different organisms belonging to three different trophic levels using the following bioassays: the inhibition of the constitutive luminescence of the bacterium *Vibrio fischeri* (decomposer), the immobilization of the microcrustacean *Daphnia magna* (primary consumer), the multigenerational growth inhibition of the green alga *Pseudokirchneriella subcapitata*, and the seed germination tests for the plants *Licopersicon esculentum*, *Lactuca sativa* and *Lolium perenne*. The bioassays represented species that could be affected by possible wastewater discharge to surface streams or by the alternative use of reclaimed wastewater for irrigation.

2. Experimental

2.1. Materials and procedure

Amine terminated G3 PAMAM-(NH₂)₃₂ dendrimer (CAS 153891-46-4) aqueous solution was purchased from Dendritech. The structure of this polymeric nanoparticle is shown in Fig. 1. The dilutions were

prepared using Milipore Mili-Q pure water (resistivity > 18 M Ω cm⁻¹ at 25°C). Phenol, ethanol (95%, v/v), sodium nitroprusside, sodium citrate and sodium hypochlorite used as described below were analytical grade reagents from Sigma–Aldrich. Methanol and acetonitrile (HPLC-grade) were supplied by Merck. Water used for LC–MS analysis was generated from a Direct-QTM 5 Ultrapure water system (Millipore). The fluorescence dyes 2',7'-dichlorofluorescein diacetate (H2DCFDA) and C4-Bodipy were obtained from Invitrogen Molecular Probes.

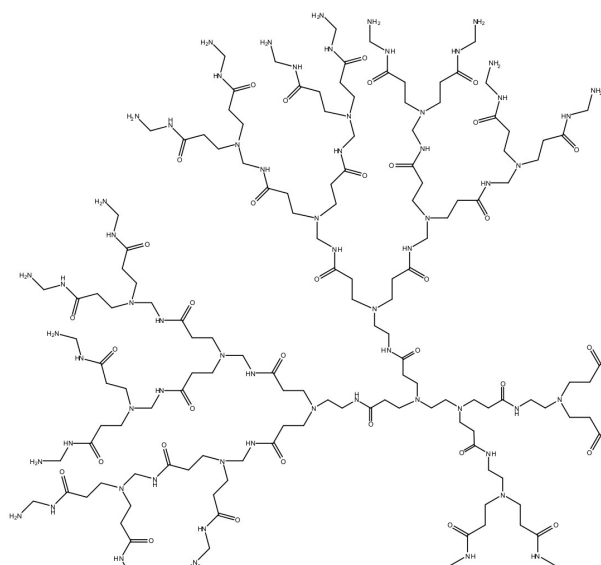


Figure 1. Structure of G3 PAMAM-(NH₂)₃₂ dendrimer.

Ozone was produced by a corona discharge and bubbled through a diffuser with a flow of 0.21 Nm³ h⁻¹ at a concentration of 12 g Nm⁻³. The ozone dosage was approximately 2 mg L⁻¹ min⁻¹, within the range usually employed for the disinfection of wastewater effluents [20]. Details are given elsewhere [21,22]. The irradiation experiments were conducted using a 15 W Heraeus Noblelight TNN 15/32 low-pressure mercury vapor lamp (254 nm) and a Heraeus TQ Xe 150 Xe-arc (visible) located inside a quartz jacketed and thermostated sleeve. In the case of visible light irradiations, an additional borosilicate glass tube was used to cut-off wavelengths <290 nm. Fluence rates per unit volume were 6.01 $\times 10^{-6}$ E L⁻¹ s⁻¹ (254 nm) for UV lamp and 1.05 $\times 10^{-6}$ E L⁻¹ s⁻¹ (290–400 nm) for Xe-arc lamp determined by chemical actinometry of hydrogen peroxide and 2-nitrobenzaldehyde for UV and Xe lamps, respectively [23,24]. All experiments were conducted at pH 7.0 \pm 0.2 and 25°C in 1.3 L vessel magnetically stirred at 900 min⁻¹.

2.2. Analyses

The structural elucidation of TP was carried out using a hybrid quadrupole time-of-flight mass spectrometer TripleTOF 5600 system (AB SCIEX) with an ESI (electrospray ionization) source coupled to an Agilent 1200 Series HPLC system (LC–ESI–QTOF–MS). It combines high resolving power and mass accuracy with a

mass range up to 40 000 Da, allowing the resolution of complex molecular structures. Details are given elsewhere [19]. The LC analysis was performed with a reversed-phase C5 analytical column (150 mm × 4.6 mm i.d. and 5 μm particle size, 300 Å, Phenomenex). Mobile phases A and B were, respectively, HPLC-grade water and acetonitrile with 5% of water, both with 0.1% formic acid. A linear gradient was set from 90% to 70% of A in 20 min, decreased up to 0% in 2 min and then maintained for 2 min. Data acquisition and processing were carried out using Analyst® TF 1.5.1 and PeakView™ (AB SCIEX) software.

Total Organic Carbon (TOC) was determined using a Shimadzu TOC-VCSH total carbon organic analyzer. Carboxylic acids, nitrite and nitrate were analyzed by means of a Dionex DX120 Ion Chromatograph equipped with a conductivity detector, a cation suppressor and a column IonPac 4 × 250 mm AS9-HC. Ammonia was measured using the method of Solorzano [25]. The concentration of ozone dissolved in the aqueous phase was measured with an amperometric Mettler Toledo 358/210 sensor and the concentration of ozone in gas phase was determined using an Anseros GM6000 photometer.

The size distribution of nanoparticles was obtained using dynamic light scattering (DLS, Malvern Zetasizer Nano ZS). Zeta potential was measured via electrophoretic light scattering in the same instrument, the measurements being conducted at 25°C in the assay media without any modification.

2.3. Toxicity determinations

The green alga *P. subcapitata* was used to conduct multigenerational growth inhibition test following the procedure displayed in OECD TG 201 open system and described elsewhere [18]. In brief, algae were cultured in OECD medium at pH 8.0 ± 0.2 and the exposed cultures were kept in 96-well microplates with a total dosed volume of 250 μL under continuous fluorescent illumination. The chlorophyll content was measured in a Fluoroskan Ascent FL plate fluorometer–luminometer.

The production of ROS was assessed at 72 h treating the cells with H₂DCFDA, the intracellular oxidation of which originates 2,7-dichlorofluorescein (DCF). 10 μL of a 10 mM H₂DCFDA stock solution was added to each well and incubated for 1 h at room temperature. C4-Bodipy was used for evaluating lipid peroxidation with a concentration of about 5 μM and 30 min incubation time. DCF and Bodipy fluorescence was recorded using a confocal fluorescence microscope (Espectral Leica TCS SP5) with excitation at 488 nm. Emissions for DCF and C4-Bodipy were recorded at 665 nm and 535 nm, respectively.

The phytotoxicity was assessed using the seed germination test for one monocotyledon *Lolium perenne* (English ryegrass) and two dicotyledons, *Licopersicon esculentum* and *Lactuca sativa* (lettuce). Certificated non-treated seeds from organic farming were used. The assays

were conducted according to US EPA procedure [26]. In brief, 5 mL of sample adjusted at pH 7.0 ± 0.2 were added to Petri dishes containing a cellulose filter paper disk. Ten sterilized (sodium hypochlorite) seeds with three replicates were placed on each disk and incubated at 23°C in the dark for six days. The test succeeded when at least 65% of control seeds germinated with roots of at least 20 mm long. The results were expressed using a germination index, $GI = (Ns/Nc)(Ls/Lc)$, where N and L are numbers of germinated seeds and average root lengths, respectively, for sample(s) and control (c) [27].

The photoluminescence inhibition of bacteria *V. fischeri* was carried out according to the ISO 11348-3 standard protocol using the commercial Biofix Lumi test (Macherey Nagel, Germany). The inhibition was measured at 16.5 ± 1.1°C in a Fluoroskan Ascent FL plate luminometer. The immobilization of *D. magna* was tested using the commercial test kit Daphtokit (Creasel, Belgium) according to the European Guideline OECD TG 202. Details for both bioassays are given elsewhere [18].

3. Results

In pure unbuffered water at pH 7.0 we observed (DLS) particles of 4.2 nm, near the size of 3.6 nm nanometer given by the producer. At larger concentrations and in the culture media the intensity signal for individual dendrimers becomes undetectable, the suspension appearing as monodisperse and formed by aggregates of a few hundreds of nanometers. This indicates that the presence of individual dendrimers coexists with relatively large aggregates, which generally hinder the former due to the similarity of the refractive indexes of PAMAM dendrimers and water. The charge of G3 PAMAM-(NH₂)₃₂ was positive in water and all culture media due to the secondary and tertiary amines forming the dendrimer structure. The results of DLS and ζ-potential measurements are given in Table S1 (supplementary information, SI).

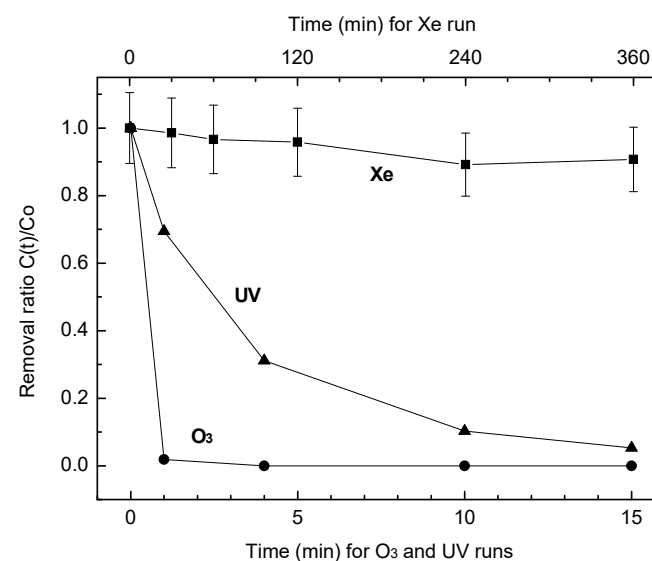


Figure 2. G3 PAMAM-(NH₂)₃₂ removal during ozone (O₃), ultraviolet (UV) and visible light irradiation (Xe).G3

PAMAM-(NH₂)₃₂ dendrimer at an initial concentration of 100 mg L⁻¹ (14.5 μM) was treated by ozone and ultraviolet and visible light irradiation. The reason for choosing this concentration was the need for a minimum concentration of transformation products to allow their analytical identification by LC-ESI-QTOF-MS and quantifying the toxic effect of their mixtures. Ozone was capable of removing +98% of dendrimer during the first minute on stream, which corresponded to an ozone dosage of 47.9 ± 4.2 μM. During the same period, UV irradiation reduced the initial concentration of G3 PAMAM-(NH₂)₃₂ by 30% (95% after 15 min). Visible light (>290 nm) irradiation resulted in low but significant (~10% for 240 min) dendrimer depletion (Fig. 2).

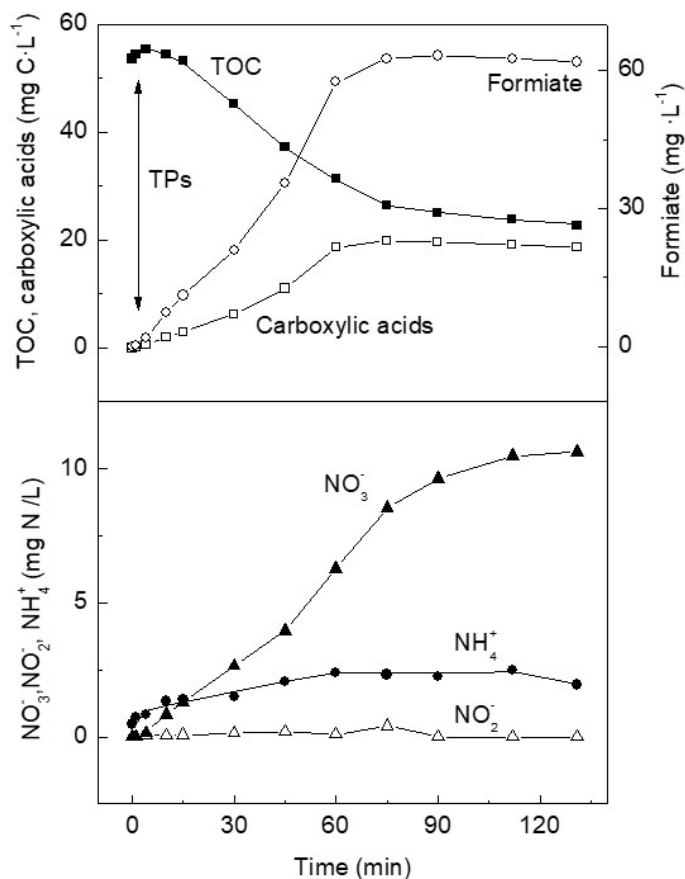


Figure 3. Nitrogen release, TOC evolution and carboxylic acids produced during the ozonation of G3 PAMAM-(NH₂)₃₂.

The evolution of TOC, carboxylic anions (formiate and oxalate) and nitrogen species (nitrate, nitrite, and ammonia) were monitored during reactions. Ozonation reached significant TOC removal after an induction period of about 15 min with TOC depletion of 50.8% for 75 min. One hour of additional treatment only led to an extra 7% removal. The concentration of carboxylic anions increased with time up to 75 min to stabilize thereafter, with an evolution parallel to TOC. Concerning nitrogen, an initial release of ammonia was observed during ozonation, its concentration increasing up to 2.4 mg N L⁻¹. Nitrite was detected in low concentration (<0.4 mg N L⁻¹) but nitrate constantly rose during the whole ozone treatment reaching more than 10 mg N L⁻¹ (Fig. 3). Considering the nitrogen content of G3 PAMAM-(NH₂)₃₂, the maximum theoretical

concentration of nitrogen would be 24.7 mg N L⁻¹. Consequently, over 40% of the total nitrogen content of the molecules was liberated as nitrate during ozonation. UV and visible light irradiation did not lead to any measurable TOC reduction or ion release.

The multiple-charging phenomenon observed in G3 PAMAM-(NH₂)₃₂ dendrimer by means of electrospray ionization provided key advantages for its identification thanks to the accurate mass measurement (below ±2.5 ppm) for the selected diagnostic ions and the assignment of elemental composition and charge state thanks to the resolution of isotopic clusters ¹³C/¹²C. Fig S1 (SI) shows a LC-ESI-QTOF-MS mass spectrum of G3-PAMAM-(NH₂)₃₂ in full scan mode, characterized by a charge state distribution of the protonated molecular ion up to +10 (MW, 3254.29). Mass error for the most abundant isotopic clusters +10, +9 and +6, selected as diagnostic ions, was in the (-2.3) - 1.9 ppm range. From all the feasible molecular formulas, ranked according mass error and ¹³C/¹²C isotope distribution, the molecular formula (C₃O₂H₆₀₈N₁₂₂O₆₀+9H)⁹⁺ was attributed to the protonated molecule [M+9H]⁹⁺ at *m/z* 768.6578 (mass error of -2.3 ppm). The isotopic distribution of [M+9H]⁹⁺ was characterized by a peak-spacing of 0.11 *m/z* unit (approx. 20,000 *fwhm*), sufficient to achieve charge state assignment. Fig. 4a shows an overlay of seven chromatograms (corresponding to the TIC, total ion chromatogram) of samples withdrawn at different times of ozonation, where the depletion of G3-PAMAM-(NH₂)₃₂ (peak at 7.5 min) and the formation of two TP are displayed. TP1 (11.0 min) showed a maximum in the signal intensity after 130 min on stream but much lower than the TP2 (13.1 min), after 4 min of treatment. Fig. 4b shows the full scan mass spectrum of TP1 and TP2 observed under ozonation. After 15 min of UV irradiation, another minor TP (TP3) was detected. The structural elucidation is discussed in the following section. It is clear that these were not the only TP obtained from irradiation and ozonation of the PAMAM dendrimer, but it was our intention to focus on those appearing in chromatograms and MS spectra with the higher intensity. Moreover, we have chosen ions that during processing time were increasing or decreasing in parallel with the evolution of the main G3 body peaks. The difficulties associated with products coming from defective ions and the molecular formula assignment in such complex and highly symmetric molecules are discussed below.

The toxicological endpoints EC50, EC20 and EC10 of G3 PAMAM-(NH₂)₃₂ are shown in Table 2. The toxic effect of G3 PAMAM dendrimer increased for the tested organisms in the following order *P. subcapitata* > *D. magna* > *L. esculentum* ≈ *L. sativa* > *L. perenne* > *V. fischeri*. Fig. 5 displays the results of the toxicity assessment of the mixtures obtained from G3 PAMAM-(NH₂)₃₂ in ozonation or irradiation assays. In samples taking along the ozonation runs, both the growth inhibition of *P. subcapitata* and the immobilization of *D. magna* initially decreased in parallel with dendrimer

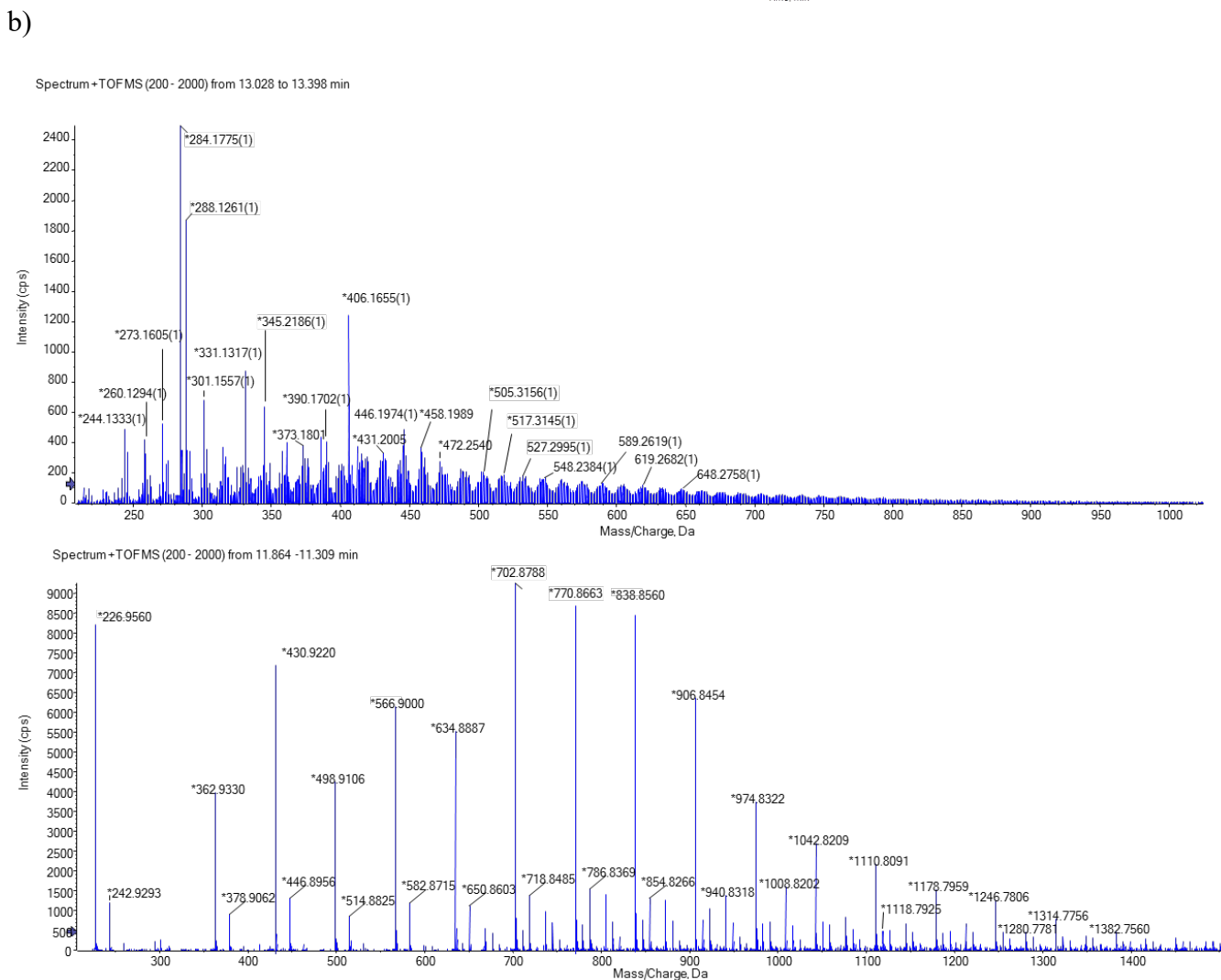
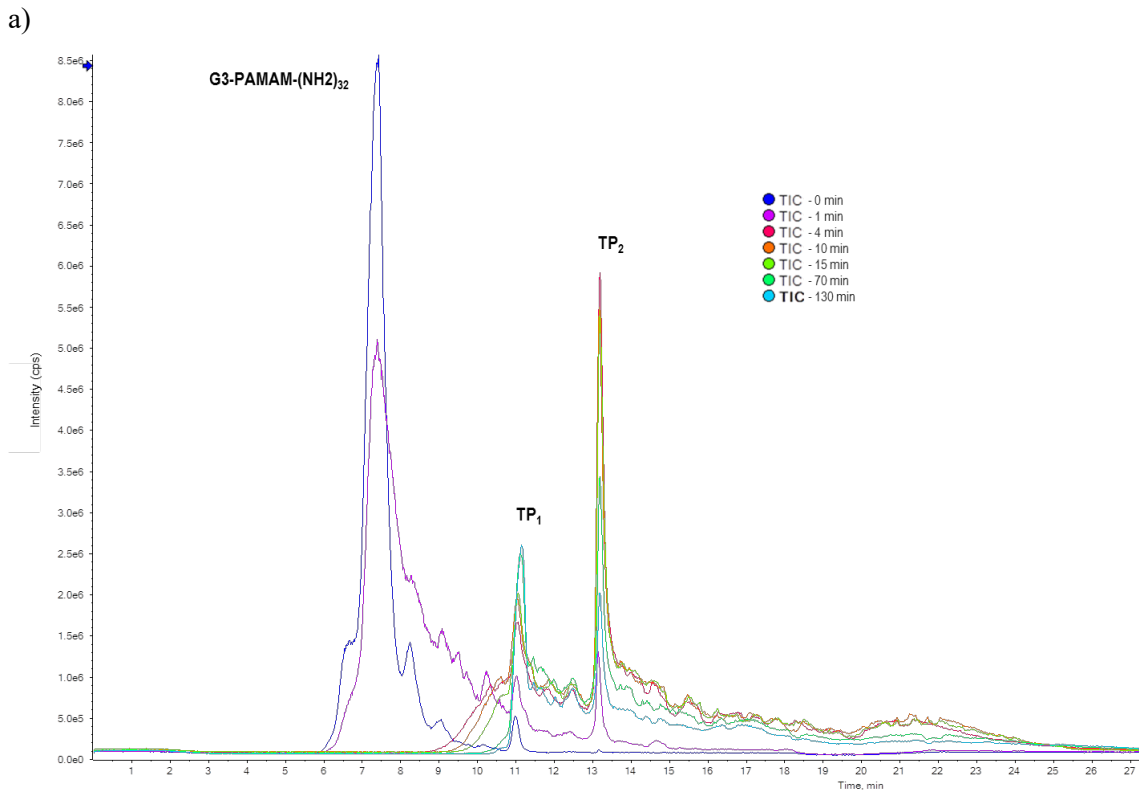
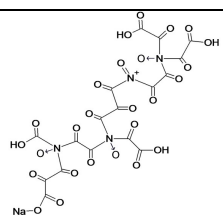
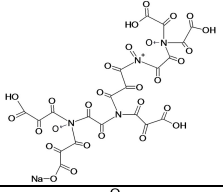
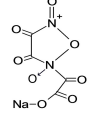
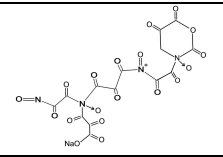
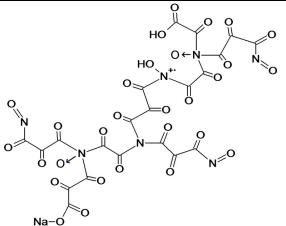
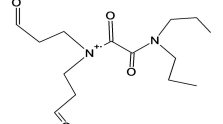
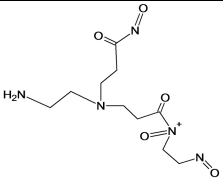
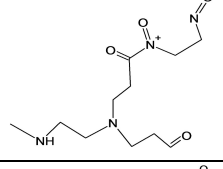
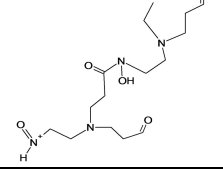
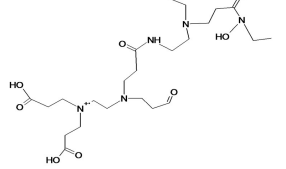
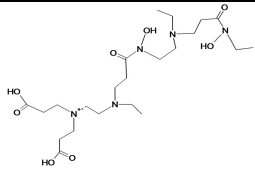
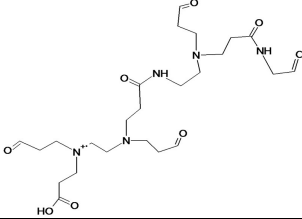
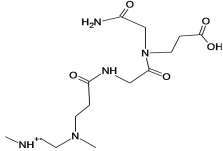
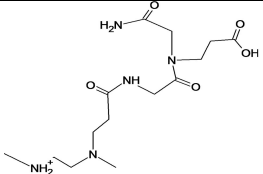
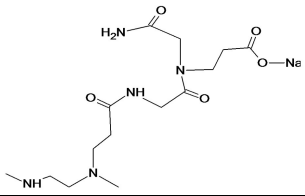
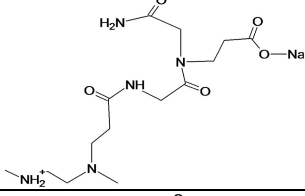
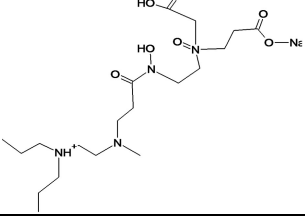


Figure 4. (a) Total ion chromatograms (TIC) of samples collected at different times of treatment (up to 130 min) showing depletion of G3-PAMAM-(NH₂)₃₂ and formation of two TP. (b) LC-ESI-QTOF-MS full scan spectrum of TP1 (130 min ozonation) and TP2 (15 min ozonation).

Table 1. Identification of transformation products (TP). TP1: ozonation, 15 min of treatment; TP2: ozonation 130 min of treatment; TP3: UV irradiation, 15 min of treatment.

TP R _t (min)	Measured mass of major diagnostic ions	Relative peak intensity (%)	Elemental composition	Calculate d mass	Error (ppm)	Proposed structures of diagnostic ions
TP1 11.00	702.8788	100	C ₁₇ H ₄ N ₄ O ₂₆ Na ⁺	702.9011	-31.7	
	770.8663	89.8	C ₂₀ H ₄ N ₄ O ₂₈ Na ⁺	770.8909	-31.9	
	226.9560	89.6	C ₄ N ₂ O ₈ Na ⁺	226.9552	3.5	
	566.9000	72.5	C ₁₄ N ₄ O ₂₉ Na ⁺	566.9003	-0.5	
	838.8560	92.1	C ₂₁ H ₂ N ₇ O ₂₉ Na ⁺	838.8794	-27.8	
TP2 13.1	284.1775	100	C ₁₄ H ₂₄ N ₂ O ₄ ⁺	284.1736	13.7	
	288.1261	65.8	C ₁₀ H ₁₈ N ₅ O ₅ ⁺	288.1307	-15.9	
	273.1605	28.3	C ₁₁ H ₂₁ N ₄ O ₄ ⁺	273.1562	15.7	
	345.2186	28.3	C ₁₅ H ₂₉ N ₄ O ₅ ⁺	345.2137	14.1	
	517.3145	12.5	C ₂₃ H ₄₃ N ₅ O ₈ ⁺	517.3111	6.5	

	505.3156	10.8	$C_{22}H_{43}N_5O_8^{+}$	505.3111	8.9	
	527.2995	10	$C_{24}H_{41}N_5O_8^{+}$	527.2954	7.7	
TP₃ 13.0	345.2078	65.5	$C_{14}H_{27}N_5O_5^{+}$	345.3954	19.1	
	346.2093	10	$C_{14}H_{28}N_5O_5^{+}$	346.2090	0.8	
	367.1890	23.3	$C_{14}H_{26}N_5O_5Na^{+}$	367.1831	16.0	
	368.1922	6.6	$C_{14}H_{27}N_5O_5Na^{+}$	368.1909	3.5	
	457.2671	5	$C_{19}H_{38}N_4O_7Na^{+}$	457.2638	7.2	

depletion. After 15 min, however, the toxicity to *D. magna* increased again up to 100% immobilization at 71 min. The opposite effect was observed for *L. sativa* and *L. esculentum*, for which a toxicity increase (GI decrease) was observed during the first part of the ozonation runs. In the case of *V. fischeri*, for which neither the dendrimer nor its transformation mixtures were particularly toxic, a certain toxicity increase was observed at intermediate times, with luminescence inhibition near 30% after 15 min. During UV irradiation, a toxicity reduction was observed for *D. magna*, with low or no effect for *P. subcapitata* and *V. fischeri*. GI for *L. esculentum* and *L. sativa* (and with less significant results for *L. perenne*) increased during the first few minutes on stream to decrease thereafter in more deeply oxidized mixtures. Visible light irradiation significantly affected *D. magna*, with 30% immobilization increase. No toxicity changes

were observed for *P. subcapitata* and *V. fischeri* and for the three plant seeds. In all cases, samples irradiated up to 6 h did not lead to significant effects on GI.

With respect to zeta potential also shown in Fig. 5, it decreased during ozonation runs from $+30.8 \pm 2.6$ mV at 0 min to -11.3 ± 1.8 mV at 15 min, dropping to -23.2 ± 1.8 mV at 131 min. Irradiation treatments kept positive zeta potential values for G3 PAMAM-(NH₂)₃₂ with minor variations during treatments. The same behavior was found for ROS production, measured by DCF fluorescence, which rapidly decreased during the first minutes of ozonation. ROS production slightly increased during UV irradiation with statistically significant data after at least 15 min of irradiation (Fig. 5). Figs. S2 and S3 (SI) show confocal microscopy images of cells of *P. subcapitata* exposed to G3 PAMAM-(NH₂)₃₂ during 72 h. Intense DCF and Bodipy signals came out as a

Table 2. Dose-Effect Relationship Parameters for the bioassays used in this work with their 95% confidence intervals. EC_x expressed in mg/L. GI: Germination Index.

	<i>V. fischeri</i>	<i>Pseudokirchneriella subcapitata</i>	<i>Daphnia magna</i>	<i>Lolium perenne</i>	<i>Licopersicon esculentum</i>	<i>Lactuca sativa</i>
EC50	-	0.41 ^a (0.39-0.43) ^a 0.15 ^b (0.13-0.17) ^b	1.45 (0.49-2.40)	259 (230-289)	191 (170-212)	185 (135-234)
EC20	833 (335- 1331)	0.23 ^a (0.20-0.26) ^a 0.078 ^b (0.058-0.098) ^b	0.231 (0.025-0.437)	169 (147-191)	117 (105-129)	123 (92-154)
EC10	100 (37-163)	0.129 ^a (0.083-0.176) ^a 0.050 ^b (0.031-0.070) ^b	0.076 (0.001-0.140)	143 (120-165)	97 (86 – 108)	108 (79-138)
Model	Log-Logistic	Log-Logistic	Log-Logistic	Brain-Cousens (hormesis) f = 0.23 ± 0.10	Brain-Cousens (hormesis) f = 0.41 ± 0.11	Brain-Cousens (hormesis) f = 1.55 ± 0.61
Notes	Conc. range: 0-1000 mg L ⁻¹ 21.9 ± 0.1% inhibition at 1000 mg L ⁻¹	Conc. range: 0-2.5 mg L ⁻¹ Microplate	Conc. range: 0-100 mg L ⁻¹	GI Conc range: 0-1000mg/L	GI Conc range: 0-1000mg/L	GI Conc range: 0-1000mg/L

^a Clear microplate (upper and lower irradiation), ^b Black bottom microplate (upper irradiation)

consequence of the production of ROS and lipid peroxidation, respectively. DCF fluorescence appeared in certain damaged cells and aggregates, which coexisted with cells with apparently no damage. C4-Bodipy fluorescence appeared at certain specific places within green algae and with high intensity in aggregates of cells and cell debris.

4. Discussion

Ozone was capable of removing +98% of dendrimer during the first minute on stream. The reaction was rapid and ozone was not detected in solution during the first 12 min. Irradiation treatments did not lead to significant mineralization, but UV irradiation removed 85% of the initial dendrimer after 10 min. The latter could be a consequence of the vacuum ultraviolet (185 nm, VUV, 15% of the total emitted power) irradiation of the lamps, which leads to the photolysis of water with subsequent formation of hydroxyl radicals [28]. This observation is further supported by the minimum overlap of G3 PAMAM-(NH₂)₃₂ absorption spectrum and lamp emission spectra as shown in Fig. S4 (SI). The maximum TOC decrease corresponds to a 57% of the initial organic carbon introduced with the dendrimer (52.4 mgC L⁻¹). The nitrogen liberated as nitrate represents 43% of the dendrimer nitrogen both figures indicating that the mineralization of organic carbon and the release of nitrogen as nitrate run in parallel as graphically displayed in Fig. 3. The rate of mineralization decreased as the reaction proceeded as shown in Fig. S5 (SI), which

displays the logarithmic decay of TOC with ozone exposure. The pseudo-second order rate constant of the ozonation process, R, fell from 32.8 M⁻¹ s⁻¹ from 15 to 45 min, approximately, to 1.1 M⁻¹ s⁻¹ for contact times over 75 min. Mineralization is not a single chemical process but represents a series of reactions that are slower for highly oxidized molecules, such as carboxylic acids. Parameter R is not constant except for a limited period of time and characterizes the progress of the ozonation process by connecting ozone profiles and TOC decay.

PeakView software was used for processing LC-ESI-QTOF-MS mass spectral data as follows: (i) selection of an ion with the highest *m/z* ratio for further molecular formula assignment, (ii) molecular formula assignment to the ions of lower *m/z* ratio and (iii) structure elucidation based on the structures proposed for diagnostic ions. Table 1 presents the empirical formulas of the diagnostic ions and the chemical structures proposed for the TP generated under ozonation and UV irradiation. Mass accuracy below ±2 ppm is generally accepted in the case of compounds of low molecular mass [30]. For chemicals of higher molecular weight there are no well-established criteria regarding mass accuracy for structural elucidation. For instance, in the analysis of peptides and proteins, the influence of mass resolution and peak shapes, gives rise to errors as high as ~10 to 100 ppm [31,32]. At least three ions with mass error below 10 ppm were required to characterize TP. To elucidate the major TP (TP2), the monocharged ions at *m/z* 505.3156 (8.9 ppm), 517.3145 (6.5 ppm) and 527.2995376 (7.7 ppm)

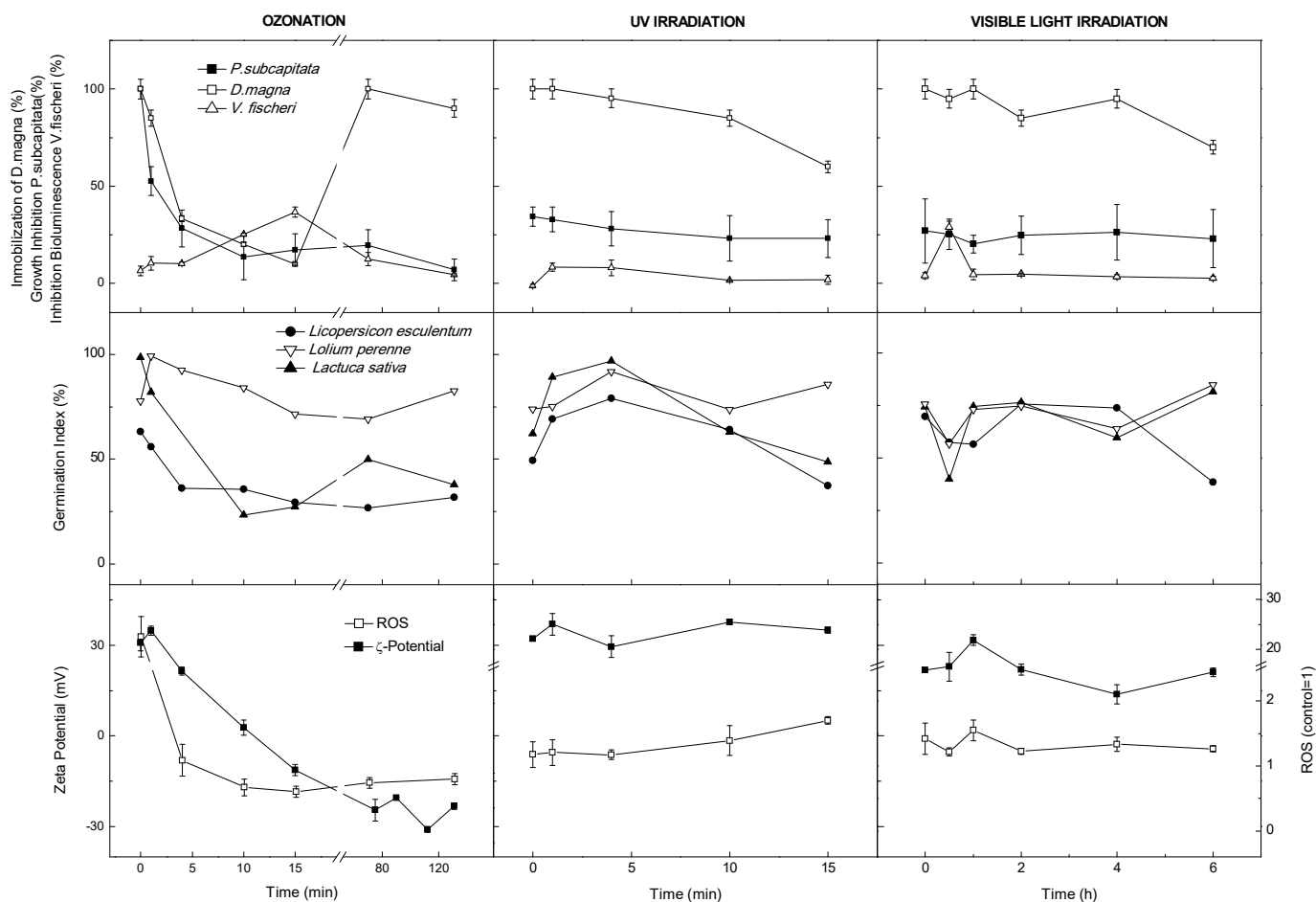


Figure 5. Toxicity assessment of ozonated and irradiated mixtures.

were selected, despite their relative intensity 10–15%, but within mass error tolerance. Additionally, the ions at m/z 273.1605378 (15.7 ppm), 284.1775 (13.7 ppm), 288.1261 (–15.9 ppm), 345.2186379 (14.1 ppm) of higher relative intensity (28–100%) were also taken into consideration. The ion at m/z 527.2995 was assigned to a unique elemental composition $C_{24}H_{41}N_5O_8^{+}$, which may lead to several structures. To overcome this constraint, a detailed examination of tentative structures stoichiometrically coherent with a polyamidoamine dendrimer, was carried out using the structure elucidation tool. MS fragmentation pattern of PAMAM from generation G0 to G3 was discussed in a previous article [33]. Most of the product ions detected using LC/ESI-QTOF-MS corresponded to neutral losses of one full amino amide branch ($C_5H_{10}N_2O$, 114 Da) and a part of this branch ($C_4H_{10}N_2O$, 102 Da), respectively. These fragments have been associated to a retro-Michael reaction, which in the case of the loss of 114 Da fragments resulted in secondary amines from tertiary ones. This is the opposite to the Michael addition reaction between primary or secondary amino groups and acrylic functional groups that take place during the synthesis of PAMAM dendrimers and has been previously described in detail [34]. The ion at m/z 527.2995 may result from hydrogen migration and α -cleavage reaction at the most exterior tertiary amines and sequential losses of amino amide branches resulting in a structure similar to a dendrimer of generation G0 with an

ethylenediamine core and a dendron of the layer corresponding to a G1. The oxidation of this structure resulted in the formation of carboxylic acids, also observed for the ions at m/z 505.3156 ($C_{22}H_{43}N_5O_8^{+}$) and 517.3145403 ($C_{23}H_{43}N_5O_8^{+}$). It has been suggested that the initiation of photooxidation of polyamides, predominantly occurs through a radical scission of the C-N bond of the amide group [35,36]. The oxidation of secondary amines and tertiary amines resulting in the formation of amine oxide is suggested by means of the ions at m/z 505.3156, 517.3145, 345.2186 ($C_{15}H_{29}N_4O_5^{+}$) and 288.1261 ($C_{10}H_{18}N_5O_5^{+}$), 273.1605 ($C_{11}H_{21}N_4O_4^{+}$), respectively. The ions at m/z 273.1605410 and 345.2186 confirmed the formation of highly oxidized intermediates affecting the ethylenediamine core.

The most plausible structure for the minor TP (TP1) formed after 130 min under ozonation, suggests a higher oxidation state. The ion at m/z 838.8560 was assigned to $C_{21}H_{27}N_7O_{29}Na^{+}$ with a mass error of –27.8 ppm. Mass error exceeding 50 ppm was obtained for any lower percentage composition of oxygen, discarding this approach. The added oxygen in the elemental composition is present mainly as carbonyl and carboxyl groups, as well as amine oxides. With better mass accuracy, the ions at m/z 226.9560 ($C_4N_2O_8Na^{+}$, 3.5 ppm) and 566.9000 ($C_{14}N_4O_{29}Na^{+}$, –0.5 ppm) also appear to be consistent with a high oxidation state and the fragmentation pattern observed in TP2. The ion at m/z

226.9560 could be associated with an intermolecular cyclization of the ethylenediamine core, reported in previous studies [19,33]. The ion at m/z 566.9000 could be rationalized assuming the formation of an anhydride from two terminal carboxyl groups. The ions at m/z 770.8663 ($C_{20}H_4N_4O_{28}Na^+$, -31.9 ppm) and 702.8788 ($C_{17}H_4N_4O_{26}Na^+$, -31.7 ppm) resulted from the ion at m/z 838.8560 due to the successive scission of the C-N bond of the amide group. Several other mono-charged species that appear in the spectrum at m/z 1110.8091, 1042.8209, 974.8322, 906.8454, 634.8887, 498.9106, 430.9220, 362.9330 did not provide acceptable mass errors for a reliable characterization. On the other hand, all those ions showed a sequential loss of 68 Da, which once more would support the formation of carboxylic acids during ozonation ($HCOONa$).

The full scan mass spectrum of TP3, the TP detected in UV irradiation runs, yielded the ions at m/z 457.2671, 368.1922, 367.1890, 346.2093 and 345.2078, which were assigned to elemental formula consistent with dendrimer composition. With a mass error of 7.2 ppm, the elemental composition $C_{19}H_{38}N_4O_7Na^+$ was assigned as the most probable for the ion at m/z 457.2671, evidencing a lower degree of oxidation, also supported with the ions 345.2078 ($C_{14}H_{27}N_5O_5^+$, 19.1 ppm), 346.2093 ($C_{14}H_{28}N_5O_5^+$, 0.8 ppm) and their respective sodium adducts 367.1890 ($C_{14}H_{26}N_5O_5Na^+$, 16 ppm), 368.1922 ($C_{14}H_{27}N_5O_5Na^+$, 3.5 ppm). Table 1 presents the proposed structures for these diagnostic ions. The formation of carboxylic acids and amine oxides could be explained again as a consequence of the VUV irradiation of the low-pressure mercury lamps.

No information exists about the toxicity of G3 PAMAM-(NH_2)₃₂ for the organisms commonly used in ecotoxicity tests and comparisons can only be established with close dendrimer generations. We found a particularly high effect for the green alga. The EC_{50} , 0.059 μM or 0.41 $mg L^{-1}$, was in good agreement with the value (1.4 $mg L^{-1}$) previously reported for G4 PAMAM [14]. For *P. subcapitata*, it was reported that EC_{50} for G1 PAMAM-(NH_2)₈ was 8.9 $mg L^{-1}$ (4.1 μM). The higher toxicity for G3 can be rationalized in terms of its positive surface charge leading to a stronger interaction with cell membranes followed by rapid internalization [37]. Naha et al. measured EC_{50} of G4 for *V. fischeri* of 44.2 $mg L^{-1}$ (3.11 μM) [38]. In this work, however, we found very low toxic effect of G3 for *V. fischeri*, with luminescence inhibition of $21.9 \pm 0.1\%$ for 1000 $mg L^{-1}$ (144.7 μM). Our result is closer to the 30 min EC_{50} reported for G2 PAMAM: 632 $mg L^{-1}$ (194 μM) [39]. Better agreement can be observed for *D. magna*, whose EC_{50} immobilization by G4 was 9.7 $mg L^{-1}$ (0.68 mM) as reported previously [38]. This result favorably compares with the EC_{50} of 1.45 $mg L^{-1}$ (0.21 μM) obtained here for G3. The toxicity of G3 PAMAM-(NH_2)₃₂ for seed germination was low, with EC_{10} in the order of 100 $mg L^{-1}$ (14.5 μM). It is interesting to note that seeds exposed at a low concentration of dendrimer resulted in GI above

control, this being particularly intense for *L. sativa*. The data are plotted in Fig. S6 (SI).

Petit et al. showed that G2–G4 amine-terminated PAMAM dendrimers stimulate the photosynthetic metabolism of the green microalga *Chlamydomonas reinhardtii* leading to the production of ROS [40]. The relationship with ROS overproduction is a consequence of the high sensitivity of the photosystem to stressors and has also been proved elsewhere [41]. Fig. S2 shows micrographs of *P. subcapitata* cells exposed to 0.5 $mg L^{-1}$ G3 PAMAM-(NH_2)₃₂ during 72 h. An intense DCF signal appeared in certain cells and in areas of cell aggregates. In general ROS distribute throughout damaged cells, which coexisted with others with no DCF signal and normal levels of chlorophyll fluorescence. Fig. S3 displays chlorophyll and C4-Bodipy micrographs obtained for the same culture. Bodipy reveals lipid peroxidation in endomembranous organelles. The signal of Bodipy appeared linked to the accumulation of aggregates of cells and cell debris in which toxic effects are apparent. Lipid peroxidation appeared at certain specific places within green algae, which seemed unrelated with chloroplasts.

Ozonated mixtures presented a toxicity increase that was particularly severe for *D. magna* (Fig. 5). Part of this toxicity enhancement could be attributed to the formation of formic acid, whose concentration rose up to 65 $mg L^{-1}$ after 130 min of ozonation (Fig. 3). This represents about half of the EC_{50} mobility inhibition for *D. magna*, which is 120 $mg L^{-1}$ [42]. Other acids did not represent a significant contribution to the total toxicity and, for example, oxalic acid was measured in concentrations as high as one tenth its EC_{50} [43]. A number of TP were obtained from the decomposition of the polymeric structure originated from C-N bond scission of the amide groups. As ozonation proceeds, the structures obtained were more oxidized and carboxylic acids and other oxygenated compounds appear. The positive charge of amino terminated dendrimers has been associated with its higher toxicity compared with their hydroxyl terminated counterparts [14].

We obtained, however, high toxicity in mixtures in which the ζ -potential was negative as a consequence of the oxidation of amine terminal groups. This is the case of ozonation after 10 min on stream as indicated in Fig. 5, the most probable cause being the formation of low molecular weight carboxylic acids, which has been recognized as particularly toxic to *D. magna* [44].

A common explanation for nanoparticle cytotoxicity starts with their internalization according to any endocytosis pathway. The internalization of polycationic dendrimers into cells may proceed through the formation of transient nano-holes in the cell membrane [45]. Damage of intracellular membranes could be the consequence of the localization of dendrimers in the mitochondria, which would lead to an increased ROS production and the disruption of the mitochondrial electron transduction chain with an additional ROS

production [46]. The toxicity of TP would be associated with the formation of low molecular weight carboxylic acids.

5. Conclusions

Amine terminated G3 PAMAM dendrimer becomes completely removed by ozone in less than 1 min while UV germicidal irradiation depletes 85% after 10 min. The most probable mechanism for the latter is a hydroxyl-mediated oxidation rather than direct photolysis. The effect of visible light (>290 nm) irradiation is much more limited (<10% after 2 h).

The extent of mineralization was limited and a number of TP appeared, some of which could be identified by LC/ESI-QTOF-MS. The suggested reaction pathway includes the oxidation of secondary and tertiary amines resulting in the formation of amine oxide and the scission of the C N bond of the amide group. The oxidation of the fragments gave rise to the formation of carboxylic acids, amine oxides and some highly oxidized TP.

Both ozonation and irradiation produce transformation products more toxic than the parent dendrimer for certain species. The toxicity increase was particularly apparent for *D. magna* in ozonated mixtures and could be attributed to the formation of low molecular weight oxidized species such as carboxylic acids, including formic acid, which was detected in concentration as high as half of its medium effect value for that organism.

The toxicity of G3 PAMAM-(NH₂)₃₂ was linked to a strong increase of intracellular ROS measured by DCF and Bodipy fluorescence. While DCF signal indicated that ROS-damaged cells coexisted with apparently normal ones, intense lipid peroxidation localized in intracellular bodies of algal cells.

Acknowledgements

This work has been financed by the Spanish Ministry of Science (CTM2008-04239/TECNO). One of the authors, JSM, thanks the Spanish Ministry of Education for the award of a FPU grant. The authors also wish to thank Soledad Gonzalo and Mar Fernández for their help in running the experiments.

References

- [1] OECD, List of Manufactured Nanomaterials and List of Endpoints for Phase One of the Sponsorship Programme for the Testing of Manufactured Nanomaterials: Revision. OECD Paris, 2010.
- [2] S. Svenson, D.A. Tomalia, Dendrimers in biomedical applications—reflections on the field, *Adv. Drug Deliv. Rev.* 57 (2005) 2106–2129.
- [3] J.R. Baker, I. Majoros, *Dendrimer-Based Nanomedicine*. Pan Stanford Publishing, Singapore, 2008.
- [4] A. Uclés, M.M. Ulaszewska, M.D. Hernando, M.J. Ramos, S. Herrera, E. García, A. R. Fernández-Alba, Qualitative and quantitative analysis of poly(amidoamine) dendrimers in an aqueous matrix by liquid chromatography–electrospray ionization–hybrid quadrupole/time-of-flight mass spectrometry (LC-ESI-QTOF-MS), *Anal. Bioanal. Chem.* 405 (2013) 5901–5914.
- [5] J.C. Roberts, M.K. Bhalgat, R.T. Zera, Preliminary biological evaluation of polyamidoamine (PAMAM) Starburst™ dendrimers, *J. Biomed. Mater. Res.* 30 (1996) 53–65.
- [6] H. Kobayashi, M.W. Brechbiel, Nano-sized MRI contrast agents with dendrimer cores, *Adv. Drug Deliv. Rev.* 57 (2005) 2271–2286.
- [7] S.S. Nigavekar, L. Sung, M. Llanes, A. El-Jawahri, T.S. Lawrence, C.W. Becker, L. Balogh, M.K. Khan, 3H dendrimer nanoparticle organ/tumor distribution, *Pharm. Res.* 21 (2004) 476–483.
- [8] K.M. Kitchens, M.E. El-Sayed, H. Ghandehari, Transepithelial and endothelial transport of poly(amidoamine) dendrimers, *Adv. Drug Deliv. Rev.* 57 (2005) 2163–2176.
- [9] A.R. Menjoge, R.M. Kannan, D.A. Tomalia, Dendrimer-based drug and imaging conjugates: design considerations for nanomedical applications, *Drug Discov. Today* 15 (2010) 171–185.
- [10] M.M. Ulaszewska, M.D. Hernando, A. Uclés, R. Rosal, A. Rodríguez, E. García-Calvo, A.R. Fernández-Alba, Chemical and ecotoxicological assessment of dendrimers in the aquatic environment, in: M. Farré and D. Barceló (Eds.), *Analysis and Risk of Nanomaterials in Environmental and Food Samples, Comprehensive Analytical Chemistry vol. 59*, Elsevier, Amsterdam, 2012, pp. 197–233.
- [11] K.M. Kitchens, A.B. Foraker, R.B. Kolhatkar, P.W. Swaan, H. Ghandehari, Endocytosis and interaction of poly (amidoamine) dendrimers with Caco-2 cells, *Pharm. Res.* 24 (2007) 2138–2145.
- [12] K. Donaldson, L. Tran, L.A. Jiménez, R. Duffin, D.E. Newby, N. Mills, W. MacNee, V. Stone, Combustion-derived nanoparticles: a review of their toxicology following inhalation exposure, *Part. Fibre Toxicol.* 21 (2005) 2–10.
- [13] S.P. Mukherjee, F.M. Lyng, A. Garcia, M. Davoren, H.J. Byrne, Mechanistic studies of in vitro cytotoxicity of poly(amidoamine) dendrimers in mammalian cells, *Toxicol. Appl. Pharmacol.* 248 (2010) 259–268.
- [14] I. Suárez, R. Rosal, A. Rodríguez, A. Uclés, A.R. Fernández-Alba, M.D. Hernando, E. García-Calvo, Chemical and ecotoxicological assessment of poly (amidoamine) dendrimers in the aquatic environment, *TrAC Trends Anal. Chem.* 30 (2011) 492–506.
- [15] G.V. Lowry, K.B. Gregory, S.C. Apte, J.R. Lead, Transformations of nanomaterials in the environment, *Environ. Sci. Technol.* 46 (2012) 6893–6899.
- [16] M. Klavarioti, D. Mantzavinos, D. Kassinos, Removal of residual pharmaceuticals from

- aqueous systems by advanced oxidation processes, *Environ. Int.* 35 (2009) 402-417.
- [17] M. Schmitt-Jansen, P. Bartels, N. Adler, R. Altenburger, Phytotoxicity assessment of diclofenac and its phototransformation products, *Anal. Bioanal. Chem.* 387 (2007) 1389-1396.
- [18] J. Santiago-Morales, M.J. Gómez, S. Herrera, A.R. Fernández-Alba, E. García-Calvo, R. Rosal, Oxidative and photochemical processes for the removal of galaxolide and tonalide from wastewater, *Water Res.* 46 (2012) 4435-4447.
- [19] M. Hernando, P. Rosenkranz, M. Ulaszewska, M. Fernández-Cruz, A. Fernández-Alba, J. Navas, In vitro dose-response effects of poly (amidoamine) dendrimers [amine-terminated and surface-modified with *N*-(2-hydroxydodecyl) groups] and quantitative determination by a liquid chromatography-hybrid quadrupole/time-of-flight mass spectrometry based method, *Anal. Bioanal. Chem.* 404 (2012) 2749-2763.
- [20] P. Paraskeva, N.J.D. Graham, Ozonation of Municipal Wastewater Effluents, *Water Environ. Res.*, 74 (2002) 569-581.
- [21] R. Rosal, A. Rodríguez, M.S. Gonzalo, E. García-Calvo, Catalytic ozonation of naproxen and carbamazepine on titanium dioxide, *Appl. Catal. B-Environ.* 84 (2008) 48-57.
- [22] J. Santiago-Morales, M.J. Gómez, S. Herrera-López, A.R. Fernández-Alba, E. García-Calvo, R. Rosal, Energy efficiency for the removal of non-polar pollutants during ultraviolet irradiation, visible light photocatalysis and ozonation of a wastewater effluent, *Water Res.* 47 (2013) 5546-5556.
- [23] I. Nicole, J. Delaat, M. Dore, J.P. Duguet, C. Bonnel, Use of UV-radiation in water treatment - Measurement of photonic flux by hydrogen peroxide actinometry, *Water Res.* 24 (1990) 157-168.
- [24] J.M. Allen, S.K. Allen, S.W. Baertschi, 2-Nitrobenzaldehyde: a convenient UV-A and UV-B chemical actinometer for drug photostability testing, *J. Pharmt. Biomed.* 24 (2000) 167-178.
- [25] L. Solorzano, Determination of ammonia in natural waters by the phenol hypochlorite method, *Limnol. Oceanogr.* 14 (1969) 799-801.
- [26] EPA, Ecological Effects Test Guidelines. OPPTS 850.4200; Seed Germination/Root Elongation toxicity Test. EPA712-C-96-154, US Environmental Protection Agency, Washington, DC, 1996.
- [27] D.P. Komilis, E. Karatzas, C. Halvadakis, The effect of olive mill wastewater on seed germination after various pretreatment techniques, *J. Environ. Manage.* 74 (2005) 339-348.
- [28] J. Thomson, F. Roddick, M. Drikas, Natural organic matter removal by enhanced photo-oxidation using low-pressure mercury vapour lamps, *Water Sci. Technol.* 2 (2002) 435-443.
- [29] R. Rosal, A. Rodríguez, J.A. Perdigón-Melón, M. Mezcuca, A. Agüera, M.D. Hernando, P. Letón, E. García-Calvo, A.R. Fernández-Alba, Removal of pharmaceuticals and kinetics of mineralization by O₃/H₂O₂ in a biotreated municipal wastewater, *Water Res.* 42 (2008) 3719-3728.
- [30] S. Lacorte, A.R. Fernández-Alba, Time-of-flight mass spectrometry applied to the liquid chromatographic analysis of pesticides in water and Food, *Mass Spectrom. Rev.* 25 (2006) 866-880.
- [31] K. Strupat, Molecular weight determination of peptides and proteins by ESI and MALDI. *Methods Enzymol.* 405 (2005) 1-36.
- [32] J.C. Joyner, K.D. Keuper, J.A. Cowan, Analysis of RNA cleavage by MALDI-TOF mass spectrometry. *Nucleic Acids Res.* 7-41(1) (2013) e2.
- [33] M.M. Ulaszewska, M.D. Hernando, A. Uclés, A. Valverde, E. García, A.R. Fernández-Alba, Identification and quantification of poly(amidoamine) PAMAM dendrimers of generations 0 to 3 by liquid chromatography-hybrid quadrupole time-of-flight mass spectrometry (LC-ESI-QTOF-MS/MS) in aqueous medium. *Rapid Commun. Mass Spectrom.* 27 (2013) 747-762.
- [34] A. Uclés, M.J. Martínez Bueno, M.M. Ulaszewska, M.D. Hernando, C. Ferrer, A.R. Fernández-Alba, Quantitative determination of poly(amidoamine) dendrimers in urine by liquid chromatography/electrospray ionization hybrid quadrupole linear ion trap mass spectrometry, *Rapid Commun. Mass Spectrom.* 27 (2013) 2519-2529.
- [35] D. Forsström, B. Terselius, Thermo oxidative stability of polyamide 6 films. I. Mechanical and chemical characterization. *Polym. Deg. Stab.* 67 (2000) 69-78.
- [36] B. Lánská, Degradation and stabilization, in: R. Puffr and V. Kubanek (Eds.) *Lactam Based Polyamides*, vol. I: Polymerization, Structure and Properties, CRC Press, Boca Raton, p. 262, 1991.
- [37] A. Mecke, D. Lee, A. Ramamoorthy, B. Orr, M. Banaszak Holl, Synthetic and natural polycationic polymer nanoparticles interact selectively with fluid-phase domains of DMPC lipid bilayers. *Langmuir* 21 (2005) 8588-8590.
- [38] P.C. Naha, M. Davoren, A. Casey, H.J. Byrne, An ecotoxicological study of poly (amidoamine) dendrimers-toward quantitative structure activity relationships. *Environ. Sci. Technol.* 43 (2009) 6864-6869.
- [39] M. Mortimer, K. Kasemets, M. Heinlaan, I. Kurvet, A. Kahru, High throughput kinetic *Vibrio fischeri* bioluminescence inhibition assay for study of toxic effects of nanoparticles. *Toxicol. in Vitro* 22 (2008) 1412-1417.
- [40] A.N. Petit, T. Debenest, P. Eullaffroy, F. Gagné, Toxicity of PAMAM dendrimers to

- Chlamydomonas reinhardtii*, *Aquat. Toxicol.* 100 (2010) 187–193.
- [41] A. Darehshouri, U. Lütz-Meindl, H₂O₂ localization in the green alga *Micrasterias* after salt and osmotic stress by TEM-coupled electron energy loss spectroscopy. *Protoplasma* 239 (2010) 49–56.
- [42] K. Vershueren, *Handbook of Environmental Data on Organic Chemicals*, Van Nostrand Reinhold, New York, pp. 146–346, 1983.
- [43] T.L. Randall, P.V. Knopp, Detoxification of specific organic substances by wet oxidation, *J. Water Pollut. Control Fed.* 52 (1980) 2117–2130.
- [44] A. Pintar, M. Besson, P. Gallezot, J. Gibert, D. Martin, Toxicity to *Daphnia magna* and *Vibrio fischeri* of Kraft bleach plant effluents treated by catalytic wet-air oxidation. *Water Res.* 38 (2004) 289–300.
- [45] S. Hong, P.R. Leroueil, E.K. Janus, J.L. Peters, M.M. Kober, M.T. Islam, B.G. Orr, J.R. Baker, M.M.B. Holl, Interaction of polycationic polymers with supported lipid bilayers and cells: nanoscale hole formation and enhanced membrane permeability. *Bioconjugate Chem.* 17 (2006) 728–734.
- [46] J.H. Lee, K.E. Cha, M.S. Kim, H.W. Hong, D.J. Chung, G. Ryu, H. Myung, Nanosized polyamidoamine (PAMAM) dendrimer-induced apoptosis mediated by mitochondrial dysfunction. *Toxicol. Lett.* 190 (2009) 202–207.

Supplementary information

Fate and transformation products of amine-terminated PAMAM dendrimers under ozonation and irradiation

Javier Santiago-Morales¹, Roberto Rosal^{1,2, ✉}, María D. Hernando³, Maria M. Ulaszewska^{2,*}, Eloy García-Calvo^{1,2}, Amadeo R. Fernández-Alba^{2,4}

¹ Department of Chemical Engineering, University of Alcalá, 28871 Alcalá de Henares, Madrid, Spain

² Advanced Study Institute of Madrid, IMDEA Agua, Parque Científico Tecnológico, 28805 Alcalá de Henares, Madrid, Spain

³ Spanish National Institute for Agricultural and Food Research and Technology - INIA, Crta. de la Coruña, km 7.5, 28040, Madrid, Spain

⁴ Pesticide Residue Research Group, Department of Hydrogeology and Analytical Chemistry, University of Almería, 04120, Almería, Spain

✉ Corresponding author: roberto.rosal@uah.es

* Current address: Department of Food Quality and Nutrition, Research and Innovation Centre, Fondazione Edmund Mach, San Michele all'Adige, Italy.

1. Further details on toxicity determinations.

All assays have been replicated in order to obtain reproducible results. A minimum of three experiments with its corresponding replicates according to OECD TG 201 (*P. subcapitata*), OECD TG 202 (*D. magna*), ISO 11348-3 (*V. fischeri*) and US EPA-OPPTS 50.4200 (Seed germination/root elongation toxicity test) was performed. Toxicity endpoints with 95% confidence limits are displayed in Table 2. Mean values for the corresponding toxicity data together with their standard deviations in ozonated and irradiated samples are provided in Figure 4. Negative and positive controls were routinely carried out. Reference substances were used as positive controls for *V. fischeri*, *P. subcapitata* and *D. magna*, except for germination tests which do not require them according to the EPA standard. All batches were checked with concentrations near the EC₅₀ of K₂Cr₂O₇, and additionally 3,5-dichlorophenol and ZnSO₄ · 7H₂O for *V. fischeri*. ZnSO₄ · 7H₂O was also used to check the stock bacterial suspension once reconstituted.

The analysis of toxicity data was performed using the add-on package 'drc' version 2.3-0 for the open source program and environment R (<http://www.r-project.org>). The best fitting of experimental data for *V. fischeri*, *D. magna* and *P. subcapitata* was the five parameter log-logistic function:

$$E(x) = c + \frac{d - c}{\left[1 + e^{b[\log(x) - \log(EC_{50})]}\right]^g} \quad [1]$$

where E(x) indicates the average response at dosage x, c and d are the lower and upper horizontal asymptotes, respectively, b the relative slope at EC₅₀ and g the asymmetry curve parameter. For plant germination bioassays, Brain and Cousens' model was chosen because of the hormesis effect observed (Fig. S6):

$$E(x) = c + \frac{d - c + fc}{1 + e^{b[\log(x) - \log(e)]}} \quad [2]$$

This model is a variation from the four-parameter log-logistic one in which $g = 1$ and where f represents the size of the hormesis effect: the larger the value the larger the hormesis effect is. This parameter is positive in the presence of hormesis. Parameters b and e have no straightforward biological meaning, while d and c retain those of Eq. 1. EC₅₀, EC₂₀, EC₁₀ and their confidence intervals (CI) were estimated using the described 'drc' packages and fitting models.

2. Characterization of nanoparticles.

Table S1. Particle hydrodynamic size determined and ζ -potential of G3 PAMAM-(NH₂)₃₂ with their 95% confidence intervals (10 μ M unless indicated otherwise).

Size (nm)	culture media			
	Water (pH 7.0)	<i>V. fischeri</i> (pH 7.0)	<i>P. subcapitata</i> (pH 8.0)	<i>D. magna</i> (pH 7.5)
without dendrimer	-	427 \pm 92	242 \pm 25	369 \pm 63
G3-(NH ₂) ₃₂	4.15 \pm 0.18 212 \pm 24 (*)	393 \pm 40	294 \pm 32	382 \pm 41
ζ -potential (mV)				
without dendrimer	-	-0.6 \pm 2.0	-7.4 \pm 1.9	+0.1 \pm 2.4
G3-(NH ₂) ₃₂	+26.9 \pm 3.4	+10.1 \pm 2.8	+16.9 \pm 3.7	+8.1 \pm 3.1

(*) 1.0 μ M

3. Additional figures

Figure S1. LC-ESI-QTOF-MS full scan spectrum of PAMAM dendrimer of third-generation G3. Resolution of isotopic cluster [M+9H]⁹⁺. ¹³C/¹²C isotopic distribution and isotopic peak spacing.

Figure S2. Confocal micrographs of *P. subcapitata* exposed for 72 h to 0.5 mg/L G3 PAMAM-(NH₂)₃₂ showing intracellular green DCF fluorescence and red chlorophyll autofluorescence

Figure S3. Confocal micrographs of *P. subcapitata* exposed for 72 h to 0.5 mg/L G3 PAMAM-(NH₂)₃₂ showing intracellular green C4-Bodipy fluorescence and red chlorophyll autofluorescence

Figure S4. G3 PAMAM-(NH₂)₃₂ absorption spectrum and Xe and UV lamp emission spectra.

Figure S5. Logarithmic decay of TOC as a function of the integral exposure to dissolved ozone. R_i represent the second order rate constants for the mineralization process.

Figure S6. Hormesis effect on seeds of *Lactuca sativa*, *Lolium perenne* and *Licopersion esculentum* (GI = Germination Index).

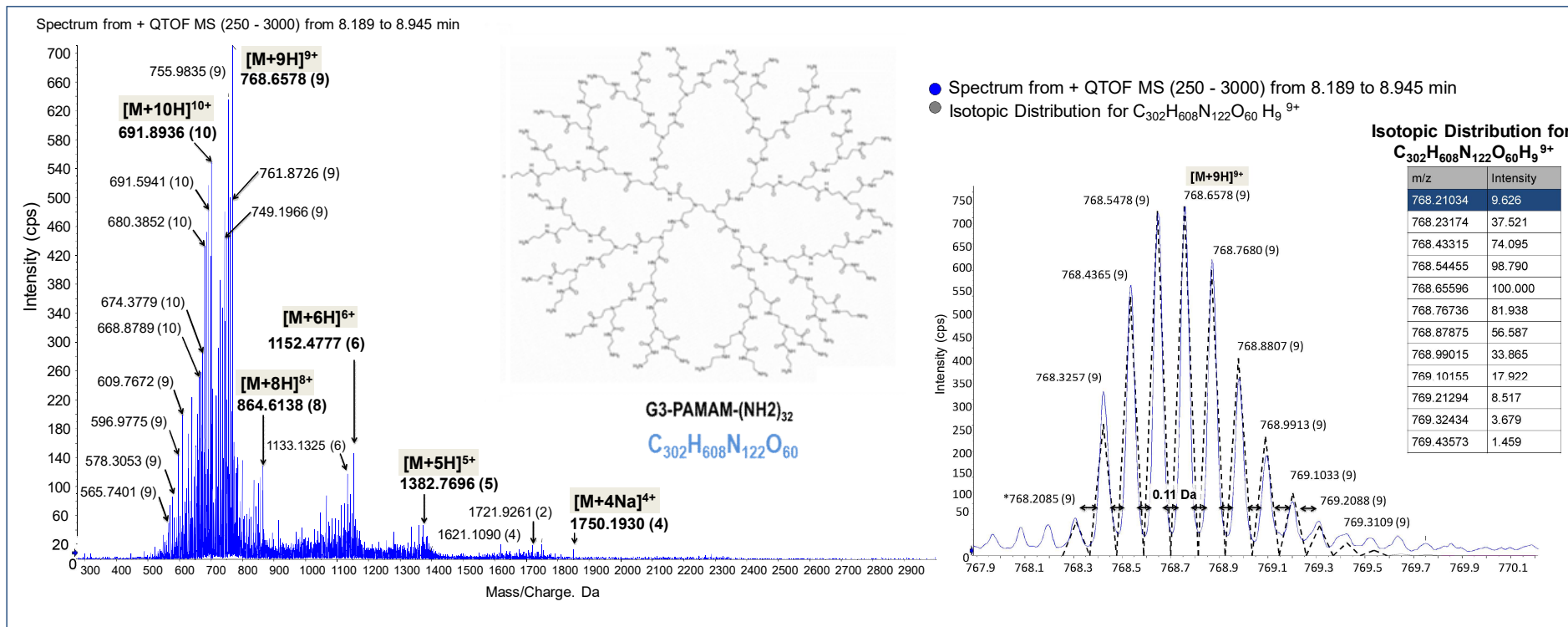


Figure S1. LC-ESI-QTOF-MS full scan spectrum of PAMAM dendrimer of third-generation G3. Resolution of isotopic cluster $[M+9H]^{9+}$. $^{13}C/^{12}C$ isotopic distribution and isotopic peak spacing.

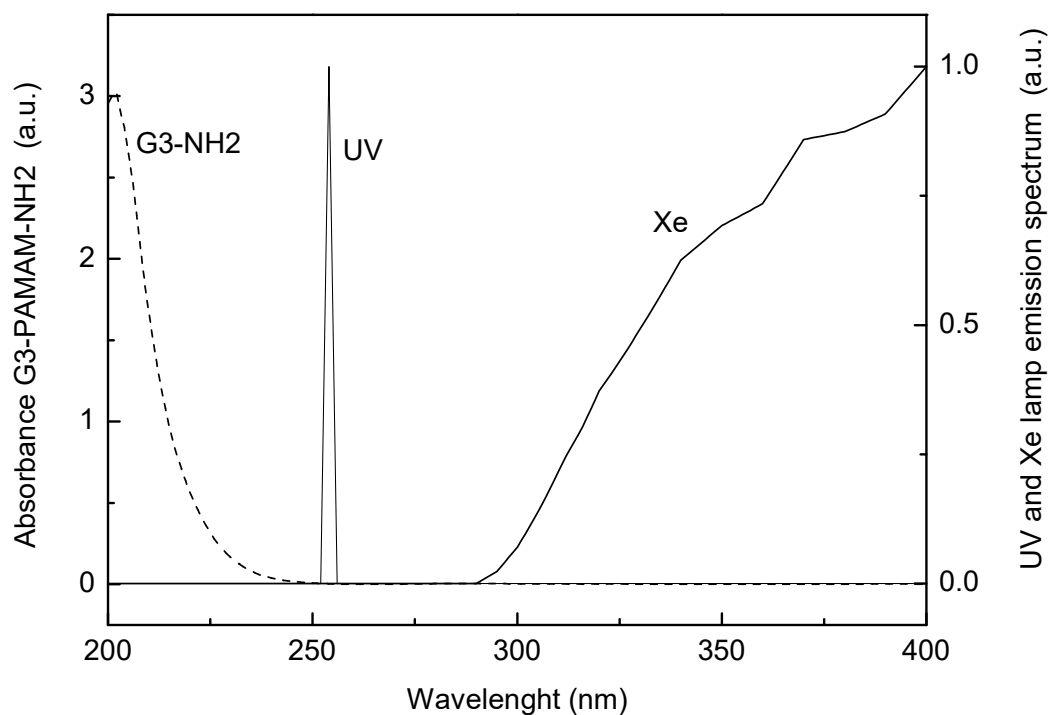


Figure S2. G3 PAMAM-(NH₂)₃₂ absorption spectrum and Xe and UV lamp emission spectra.

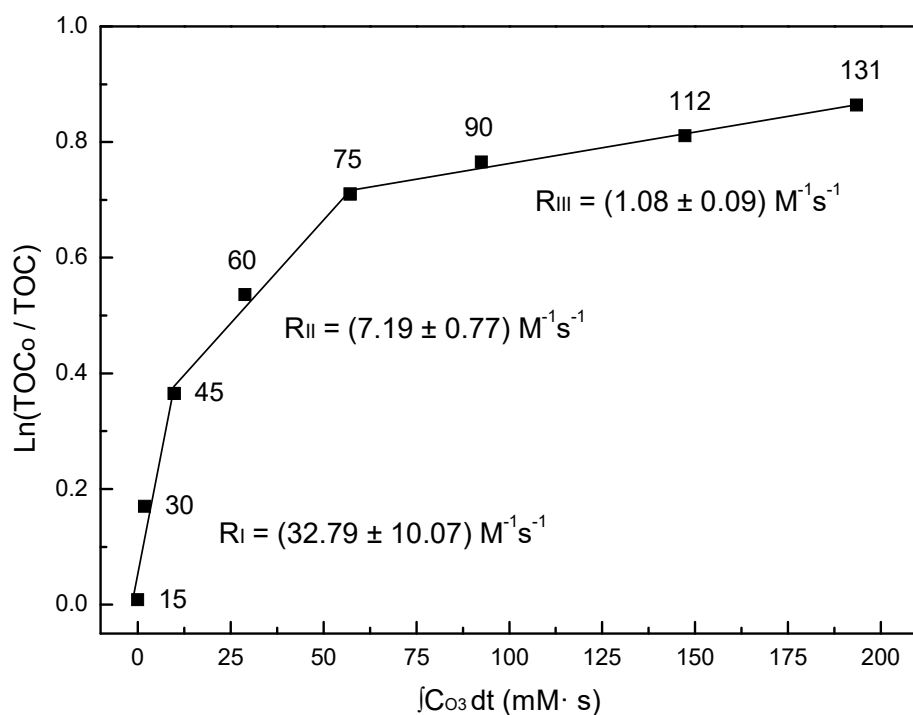


Figure S3. Logarithmic decay of TOC as a function of the integral exposure to dissolved ozone. R_i represents the second order rate constants for the mineralization process.

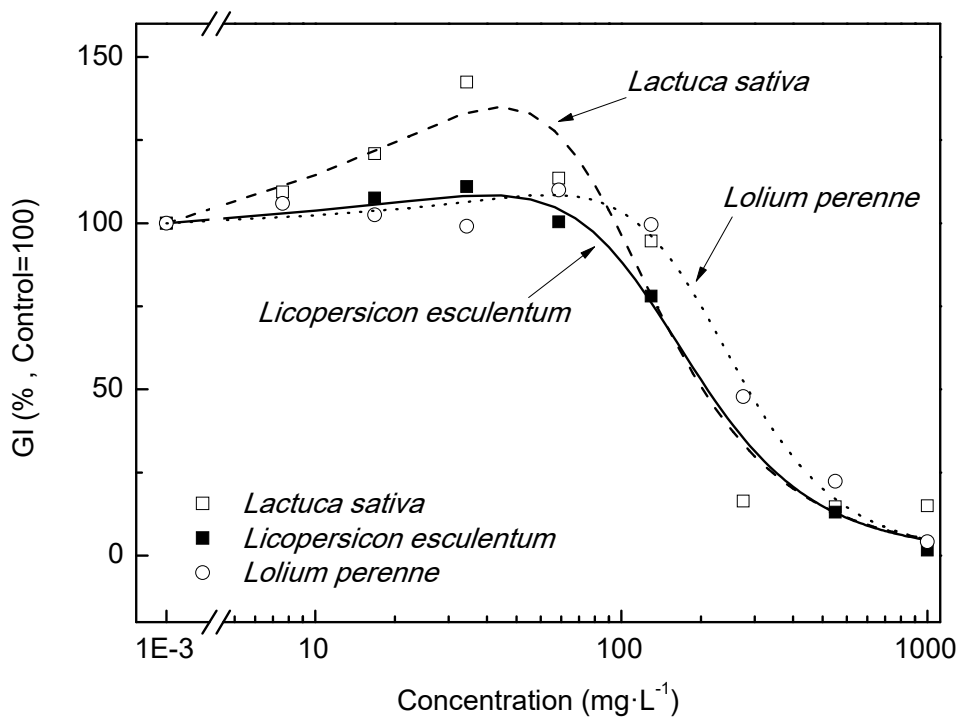


Figure S4. Hormesis effect on seeds of *Lactuca sativa*, *Lolium perenne* and *Lycopersicon esculentum* (GI = Germination Index).

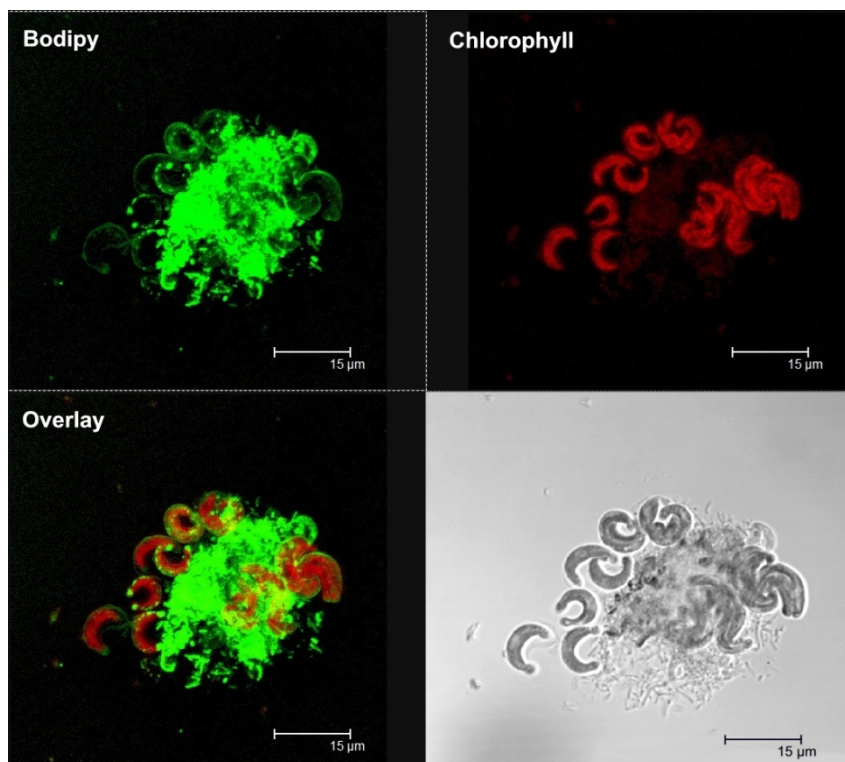


Figure S5. Confocal micrographs of *P. subcapitata* exposed for 72 h to 0.5 mg/L G3 PAMAM-(NH₂)₃₂ showing intracellular green DCF fluorescence and red chlorophyll autofluorescence

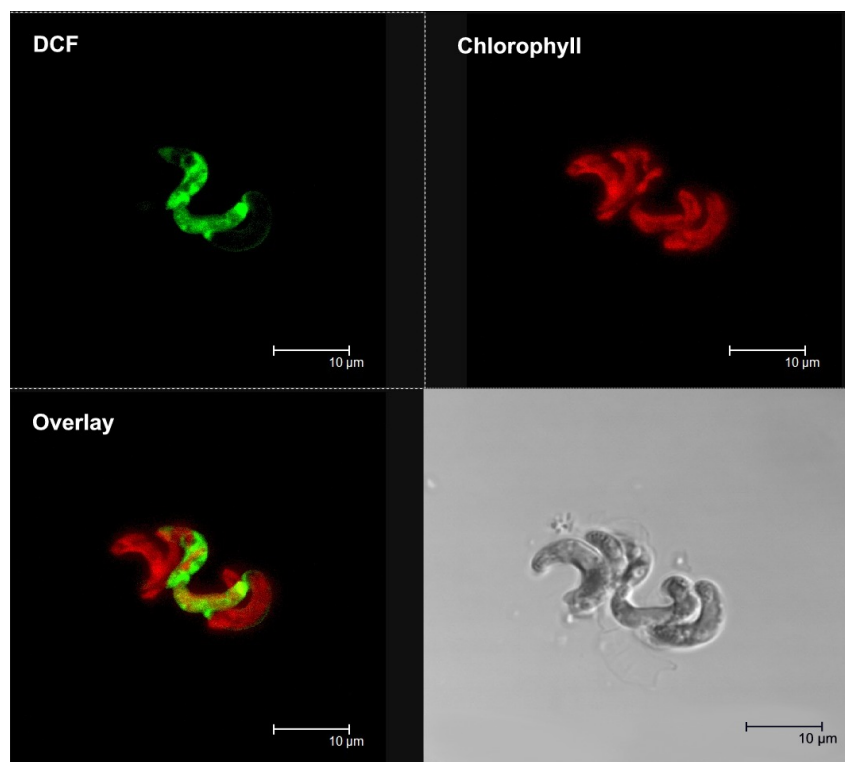


Figure S6. Confocal micrographs of *P. subcapitata* exposed for 72 h to 0.5 mg/L G3 PAMAM-(NH₂)₃₂ showing intracellular green C4-Bodipy fluorescence and red chlorophyll autofluorescence